JGR Atmospheres

RESEARCH ARTICLE
10.1029/2019JD031372

A Decadal Climatology of Chemical, Physical, and Optical Properties of Ambient Smoke in the Western and Southeastern United States

Qijing Bian[1], Bonne Ford[1], Jeffrey R. Pierce[1], and Sonia M. Kreidenweis[1]

[1]Department of Atmospheric Science, Colorado State University, Fort Collins, CO, USA

Abstract Biomass burning is a major source of summertime fine particulate matter in the United States, degrading air quality and affecting human health and climate. Fuels, burn conditions, and fire types vary across the United States, which may impact smoke composition and optical properties. We use the Hazard Mapping System to track smoke plumes for 10 years from 2008 to 2017, focusing on three U.S. regions: Southeast, Pacific West, and Southwest. Combining this geospatial data set with AErosol RObotic NETwork (AERONET) columnar data, and Interagency Monitoring of Protected Visual Environments (IMPROVE) network in situ observations, we define "smoke-influenced days" and derive the properties of smoke aerosol for April through September, encompassing the main fire seasons across the United States. We find in the IMPROVE surface measurement that the elemental carbon fraction of smoke in the Southeast is statistically different from and lower than that in the west, consistent with more-smoldering prescribed fires in the southeast. We find in the AERONET columnar observations that the mean single scattering albedo of smoke (at 675 nm) is lower in the two western regions (~0.94) compared to the southeast (~0.96), consistent with the differences in composition and fire types, which implies that the compositional differences at the surface may be representative of the column. Higher relative humidity in the southeast and less dust associated with smoke also appear to contribute to the higher smoke single scattering albedo relative to the west. Our results show that smoke properties vary regionally, with implications for models, data assimilation, and remote-sensing.

Key Points:
- We derive long-term mean smoke chemical and optical properties across three regions of the United States
- Smoke in the southeastern United States has higher sulfate content and single scattering albedo than smoke in the western United States
- Burn conditions, relative humidity, and dust coemitted with smoke may drive the variability in smoke properties between regions

Supporting Information:
- Supporting Information S1

Correspondence to:
J. R. Pierce and S. M. Kreidenweis,
jeffrey.pierce@colostate.edu;
sonia@atmos.colostate.edu

Citation:
Bian, Q., Ford, B., Pierce, J. R., & Kreidenweis, S. M. (2020). A decadal climatology of chemical, physical, and optical properties of ambient smoke in the western and southeastern United States. *Journal of Geophysical Research: Atmospheres*, *125*, e2019JD031372. https://doi.org/10.1029/2019JD031372

Received 18 JUL 2019
Accepted 20 DEC 2019
Accepted article online 26 DEC 2019

Author Contributions:
Conceptualization: Qijing Bian, Bonne Ford, Jeffrey R. Pierce, Sonia M. Kreidenweis
Data curation: Qijing Bian, Bonne Ford
Formal analysis: Qijing Bian, Bonne Ford
Funding acquisition: Jeffrey R. Pierce, Sonia M. Kreidenweis
Investigation: Qijing Bian, Bonne Ford
Methodology: Qijing Bian, Bonne Ford, Jeffrey R. Pierce, Sonia M. Kreidenweis
Project administration: Jeffrey R. Pierce, Sonia M. Kreidenweis
Resources: Jeffrey R. Pierce, Sonia M. Kreidenweis
Software: Qijing Bian, Bonne Ford
(continued)

1. Introduction

Landscape fires (wild, prescribed, and agricultural fires) are a major source of fine-mode particles. The U.S. National Emissions Inventory created by the U.S. Environmental Protection Agency estimates that these fires contribute 34% of the total primary $PM_{2.5}$ (particulate matter with aerodynamic diameters smaller than 2.5 μm) emitted in the United States (NEI, 2014). Fire-emitted particles are harmful to human health (Cascio, 2018; Crouse et al., 2012; Gan et al., 2017; Johnston et al., 2012; Liu et al., 2015; Reid et al., 2016; Yao et al., 2018), visibility (Bond et al., 2013; Brewer & Moore, 2009; Ford et al., 2018), and ecosystems (Abram et al., 2003; Sundarambal et al., 2010). Due to climatic and socioeconomic changes, wildfire activities, including the number of large wildfires, total burned areas of large wildfires, wildfire durations, and wildfire seasons, have increased in recent decades (Dennison et al., 2014; Westerling et al., 2006). Wildfire burned area, the number of large fires, fire-emitted $PM_{2.5}$, and the length of the fire season are all projected to continue to increase in the United States (Spracklen et al., 2009; Ford et al., 2018; Yue et al., 2013). Thus, landscape fires could become a larger source of fine-mode particles in the future and have increasing impacts on health and the environment.

In addition, smoke from landscape fires can also have an impact on the global radiation budget. However, there is large uncertainty in estimates of the radiative effect. Microphysical and optical properties, including aerosol size, mass extinction coefficients, single scattering albedo (SSA), and Ångström absorption exponent are important parameters in radiative effect estimates (McComiskey et al., 2008; Ramanathan et al., 2001; Ramnarine et al., 2019). A smoke SSA < 1 at a particular wavelength means that the smoke particles have some ability to absorb, and not only scatter, radiation at that wavelength, and hence the value of SSA (along with the total optical depth of the smoke plume) influences solar radiation absorption, the atmospheric radiative heating rate, and the atmospheric stability (Robock, 1988; Wang & Christopher, 2006). As an aerosol layer overlying a cloud deck, smoke can also exert above-cloud aerosol radiative impacts that are sensitive to the smoke SSA (de Graaf et al., 2012). A better understanding and representation of smoke properties

Supervision: Jeffrey R. Pierce, Sonia M. Kreidenweis
Validation: Qijing Bian, Bonne Ford
Visualization: Qijing Bian
Writing - original draft: Qijing Bian
Writing – review & editing: Qijing Bian, Bonne Ford, Jeffrey R. Pierce, Sonia M. Kreidenweis

is essential to reducing uncertainty in the estimates of the impact of smoke on the radiation budget, both in the present day and in determining how the budget may change in the future with more landscape fires.

Related to the importance of smoke properties in estimating the Earth's radiative budget, satellite retrievals of aerosol loading (e.g., aerosol optical depth, AOD) often require assumed smoke aerosol property models. Errors in these smoke property models can lead to errors in satellite aerosol retrievals and in data assimilation of aerosol characteristics. Loría-Salazar et al. (2016) showed that the MODIS Deep-Blue algorithm cannot estimate smoke-influenced AOD accurately in the semiarid western United States (r^2 between 0 and 0.31 for MODIS versus AEROENT AOD during fire periods) and hypothesized that incorrectly assumed aerosol optical properties contributed to bias in the retrieval. Shi et al. (2019) improved AOD retrievals for smoke from Indonesian fires by combining aerosol optical properties derived from AERONET data with the MODIS Dark Target (DT) aerosol algorithm.

While uncertainties in smoke optical properties influence the performance of climate models and remote sensing techniques, there are also regional differences in landscape fire types, fuels, combustion conditions, and meteorology that may impact the smoke properties. Most of the total burned area in the western United States is due to wildfires caused by lightning or human ignitions (Brey, Barnes, et al., 2018); while most of the total burned area in the southeastern United States (SE) is attributed to prescribed or agricultural burns (Melvin, 2015; Mitchell et al., 2014). Previous laboratory experiments found that the smoke produced from fuels collected in the SE had a different chemical composition than the smoke from fuels collected in the western United States (Burling et al., 2010; Levin et al., 2010; May et al., 2014; McMeeking et al., 2009). Combustion conditions (i.e., flaming through smoldering) also impact smoke emission factors, chemical composition (e.g., organics, black carbon, and potassium, McMeeking et al., 2009; Lee et al., 2010; Levin et al., 2010; Jen et al., 2019], size, and optical properties (McMeeking et al., 2014). Reid, Eck, et al. (2005) concluded that flaming, which occurs more in wildfires than in prescribed fires, produces aerosol that is more absorbing and has a lower SSA (the ratio of scattering to total extinction) compared with aerosols produced from smoldering combustion. Hence, fresh smoke in the west, if dominated by wildfires, may be more absorbing (lower SSA) than in the SE. These two regions also have different meteorological conditions that could impact the smoke properties. Malm and Schichtel (2013) showed that in the summertime, relative humidity (RH) is low in the western United States with little to no hygroscopic growth, while RH is usually higher than 80% in the SE with more than half of the particle volume being water. The additional aerosol water in the SE impacts particle size, composition, and optical properties of aerosols, including smoke (Kreidenweis et al., 2008). Hand et al. (2017) showed that fine dust concentrations are high in the southwestern United States in spring and summer due to abundant local dust sources. The arid soils in this region may lead to more dust being lofted in and around the fires by updrafts, and thus, the coemission of dust/ash could influence the chemical and physical properties of smoke (Lindsey et al., 2010; Peterson et al., 2018; Wagner et al., 2018). Given that there are different fire types, emissions, meteorological, and environmental conditions in the northwestern, southwestern, and southeastern regions of the United States, we hypothesize that there should also be different smoke properties from the fires in these different regions.

Previous work has shown that AErosol RObotic NETwork (AERONET) Sun photometer data can be used to retrieve columnar aerosol properties during smoke-influenced periods. Eck et al. (2009) examined boreal-fire aerosol properties during smoke-influenced days in Alaska and noted that SSA increased when AOD increased from 0.1 to 0.3 and hypothesized that periods of relatively thick smoke may have been associated with smoldering combustion. In addition to combustion type impacting the SSA, Sayer et al. (2014) found different SSA ranges for different fuel types (~0.95–0.97 for forest or peat burning and ~0.88–0.9 for grass, shrub, or crop burning). Some work has tried to identify specific regional differences in aerosol optical properties on smoke-influenced days using observational data. Dubovik et al. (2002) summarized AERONET inverted optical properties for smoky days in four regions: Amazonian Forest, South American Cerrado, African Savanna, and Boreal Forest and found different optical properties between the regions that they attributed mainly to differences in the average combustion conditions between regions, for example, SSA was high in smoldering burns and low in flaming burns; the fraction of these conditions varied between regions. Nikonovas et al. (2015) focused on the aging of aerosol properties in smoke plumes from northern temperate and boreal forests. They found that aging between fresh (aging time < 24 hr) and older (aging time > 72 hr) plumes increased particle size (which decreases the Ångström exponent), with an insignificant change in SSA. Shi et al. (2019) extended the study of smoke aging to the whole globe and compared

smoke-influenced aerosol from burning of different vegetation types (i.e., forest and peat versus grass and shrub). They found that particle size and SSA increased with plume age from both vegetation types. They also drew similar conclusions to Sayer et al. (2014), finding that smoldering conditions in forest and peat fires produced larger particles with less black carbon (1.08% in volume fraction), while the flaming conditions in shrub and grass fires generated smaller particles with more black carbon (3.83%). To track the smoke plumes, Eck et al. (2009) and Sayer et al. (2014) filtered smoky versus nonsmoky observations by using certain AOD cutoff values. Nikonovas et al. (2015) and Shi, Cheng, et al. (2019) determined smoke origin and age from satellite products and back trajectories. However, neither of these studies discussed the distinct vegetation differences across the United States, and all the previous studies presented properties for the total aerosol in the column (including the nonsmoke aerosol).

Ground-based observations of the chemical composition of smoke plumes have also been used, along with aircraft measurements, to investigate plume composition and changes with aging (e.g., Collier et al., 2016). However, we are only aware of one study that quantifies a climatology of ambient smoke aerosol composition through long-term surface-based observations (Schlosser et al., 2017). Schlosser et al. (2017) used long-term observations of Interagency Monitoring of Protected Visual Environments (IMPROVE) $PM_{2.5}$ speciation over the United States to analyze more than 40 fire cases in the western United States They showed that smoke-impacted measurements are associated with dust enhancement, chloride depletion, and enhancement of some other elements (P, K, nitrate, and Zn) along with the expected enhancements of carbonaceous species. However, similar to the remote-sensing studies described above, Schlosser et al. (2017) did not isolate the smoke properties from the nonsmoke aerosol, and they only focused on large wildfires in the western United States

As atmospheric aerosols are generally impacted by multiple sources (e.g., dust, sea salt and anthropogenic emissions), isolating the contribution of individual sources to observed aerosol properties is challenging. Brey, Ruminski, et al. (2018) and O'Dell et al. (2019) demonstrate the usefulness of a satellite analysis product, the Hazard Mapping System Fire and Smoke Product (HMS), to identify the locations of smoke plumes and determine smoke impacted days and regions. We summarize the relevant characteristics of the HMS smoke product here. To create HMS smoke polygons, analysts rely on visible satellite images; thus, it may be difficult to distinguish between smoke and cloud or smoke and anthropogenic haze. The visible satellite images are only available during daylight hours. Analysts release the product between 8 and 10 a.m. eastern time every day and then update it throughout the day as time permits and more satellite data become available. This update can occur every hour or more during the afternoon and early evening during fire-burning periods (Ruminski et al., 2006); we use the intersection with any of the daily posted HMS data to identify a smoke event at our sites. However, nighttime-only smoke events will be missed, but could be captured in the IMPROVE samples. Short-lived smoke events could also be missed, especially when they occur out of season as the updates are less frequent. Therefore, HMS smoke polygons provide a conservative estimate of the occurrence of smoke plumes. In addition, another limitation is that the HMS product does not provide any information on the vertical distribution of smoke, just the horizontal extent of the plume. In this study, we extend the methods of Brey, Ruminski, et al. (2018) and O'Dell et al. (2019) to locate smoke plumes and then isolate smoke properties using the differences in aerosol properties between days with and without smoke impacts over a full decade of observations. We estimate smoke properties (chemical composition and optical properties) using columnar and surface in situ measurements, and we evaluate how these properties vary across the western and SE United States—regions heavily impacted by fires, and for which we hypothesize that smoke properties may differ due to differences in fuels, fire type, and meteorology.

2. Methods and Data Processing

Wildfires and prescribed fires in the United States occur primarily in the spring, summer, and fall. However, there are other biomass burning emission sources throughout the year; for example, wood burning for residential heating is common in many regions in the wintertime (Sullivan et al., 2019). To avoid interference from wintertime residential burning, we only select data from 1 April to 30 September, for 10 years spanning from 2008–2017. We study the aerosol properties using AERONET (https://aeronet.gsfc.nasa.gov/) and IMPROVE (http://vista.cira.colostate.edu/Improve/) data.

The AERONET network provides direct-Sun measurements of spectral AOD and almucantar inversion aerosol products for four wavelengths (440, 675, 870, and 1,020 nm; Giles et al., 2019] from surface-based columnar measurements around the globe. The parameters that we use in this study include: AOD, absorption aerosol optical depth (AAOD), extinction Ångström exponent (EAE, λ_1/λ_2, equation (1), where λ_1 and λ_2 are the different wavelengths), absorption Ångström exponent (AAE, λ_1/λ_2, equation (2)), and aerosol volume size distribution (22 bins), along with the size distribution bimodal parameters, refractive index, and single scattering albedo. We use the Version 3, Level 1.5 cloud-screened and quality-controlled direct-Sun and inversion products. For reference, the Ångström exponents are computed as follows:

$$EAE(\lambda_1/\lambda_2) = -\frac{\ln(AOD(\lambda_1)) - \ln(AOD(\lambda_2))}{\ln(\lambda_1) - \ln(\lambda_2)} \quad (1)$$

$$AAE(\lambda_1/\lambda_2) = -\frac{\ln(AAOD(\lambda_1)) - \ln(AAOD(\lambda_2))}{\ln(\lambda_1) - \ln(\lambda_2)} \quad (2)$$

The IMPROVE network monitors particulate matter composition at over 100 sites in national parks and wilderness areas across the United States They collect 24-hr samples every 3 days, which are analyzed for total gravimetric mass ($PM_{2.5}$ and PM_{10}), as well as carbonaceous, ionic, and metal mass concentrations. In this study, we use the following chemical species: elemental carbon (EC), organic carbon (OC), nonsoil potassium (KNON), silicon (Si), coarse particle (PM_{10}–$PM_{2.5}$), $PM_{2.5}$, nitrate, and sulfate. We estimate organic matter (OM) from [OC] × 1.5, following the biomass burning study of Levin et al. (2010). Soil is calculated by the following equation (Malm et al., 1994):

$$[\text{Soil}] = 2.2\times[Al] + 2.49\times[Si] + 1.63\times[Ca] + 2.42\times[Fe] + 1.94\times[Ti] \quad (3)$$

Nonsoil K is calculated by the equation from Gebhart et al. (2001).

$$[\text{KNON}] = [K] - 0.6[Fe] \quad (4)$$

To examine the possible effect of water uptake on particle optical properties, we use the daily average RH data at the surface for April through September 2017 from the NOAA U.S. Climate Reference Network/U.S. Regional Climate Reference Network (USCRN/USRCRN) data product (ftp://ftp.ncdc.noaa.gov/pub/data/uscrn/products/daily01/).

The Hazard Mapping System Fire and Smoke Product (HMS) is an analysis product that tracks fire locations and smoke plumes in North America using satellite imagery (Rolph et al., 2009). Similar to O'Dell et al. (2019) and Brey, Ruminski, et al. (2018), we flag data as "smoky" when the AERONET sites are overlapped by an HMS smoke polygon. There are several limitations to using the HMS product to determine when smoke may be present in surface observations, as noted in O'Dell et al. (2019). The HMS data set only provides the horizontal extent of the smoke plumes and does not identify the altitude of smoke plumes in the atmospheric column. Therefore, in order to ensure that smoke is at the surface for analyses using IMPROVE data, we further constrain those smoky days to when the $PM_{2.5}$ concentration is greater than the mean plus 1 standard deviation (σ), determined from all the days in the study period (April–September each year), in addition to the requirement for overlap by an HMS smoke polygon. We also test a total carbon (TC) criterion that selects smoky days as those for which the TC concentration is greater than the mean plus one standard deviation (σ) (computed for that year of data) to see if the different criteria lead to different conclusions. Because AERONET provides column measurements, we do not apply this additional constraint for our AERONET analyses. We list the number of data points for smoky and nonsmoky days for the different observations and regions in Table 1. From the table, we note that the differences in the number of identified smoky days at the surface, between the $PM_{2.5}$ and TC criteria, is at most 15%.

To distinguish the regional differences in smoke properties, we separate our data set into three regions. Brey, Barnes, et al. (2018) discussed the different environmental and meteorological conditions that influence landscape fires in the western and southeastern United States, respectively. However, we further divide the western region into the Pacific West (PW) and the (non-California) southwest (SW) due to the different environmental conditions (primarily, whether the region is dust-prone or not, as mentioned in Hand et al.,

Table 1
Numbers of IMPROVE and AERONET Data Points Used in the Study

Region	Group	IMPROVE	AERONET
Pacific West	nonsmoky	27,750	34,187
	HMS-overlap smoky days[a]	5,072	7,135
	+$PM_{2.5}$ criterion[b]	1,718	
	+TC criterion[c]	1,733	
Southwest	non-smoky	15,629	36,835
	HMS-overlap smoky days	1,110	5,002
	+$PM_{2.5}$ criterion	447	
	+TC criterion	497	
Southeast	non-smoky	7,368	11,451
	HMS-overlap smoky days	371	1,148
	+$PM_{2.5}$ criterion	110	
	+TC criterion	126	

[a]HMS-overlap criterion for smoky days: Numbers are the total counts of days/sites with both valid data and that are within an HMS polygon. [b]$PM_{2.5}$ criterion for smoky days: Numbers are the counts of days/sites with $PM_{2.5}$ > mean + 1 standard deviation (σ) at that site in the corresponding year, to capture days when the smoke plume is at the surface. [c]TC criterion for smoky days: Count of days with TC > mean + 1 standard deviation (σ) at that site in the corresponding year, assuming that high TC concentrations are associated with the presence of smoke.

2017). Figure 1 is a map of our three regions and the locations of the AERONET and IMPROVE sites that we used. We include California in the PW considering that some of the observation sites in CA are near the coast and in northern California, possibly sharing the same characteristic of background aerosol and meteorological condition with Oregon and Washington.

O'Dell et al. (2019) estimated smoke $PM_{2.5}$ contribution as the difference between the daily mean $PM_{2.5}$ concentration on smoky days and the seasonal-mean $PM_{2.5}$ concentration of the days without an HMS polygon (nonsmoky). We apply a similar approach in our study. Smoke chemical composition (denoted by $species_{smoke}$), smoke AOD (AOD_{smoke}) and smoke AAOD ($AAOD_{smoke}$) are estimated by the difference between the mean values of these properties on smoky versus non-smoky days in the three regions through equations (5)–(7). Smoke optical properties including EAE_{smoke}, AAE_{smoke} and SSA_{smoke} are estimated using equations (8)–(10).

$$[species_{smoke}] = \left[\overline{species_{smokyday}}\right] - \left[\overline{species_{nonsmokyday}}\right] \quad (5)$$

$$AOD_{smoke,i} = \overline{AOD_{smokyday,i}} - \overline{AOD_{nonsmokyday,i}}, i = 440, 675, 870, \text{and } 1,020 \text{ nm} \quad (6)$$

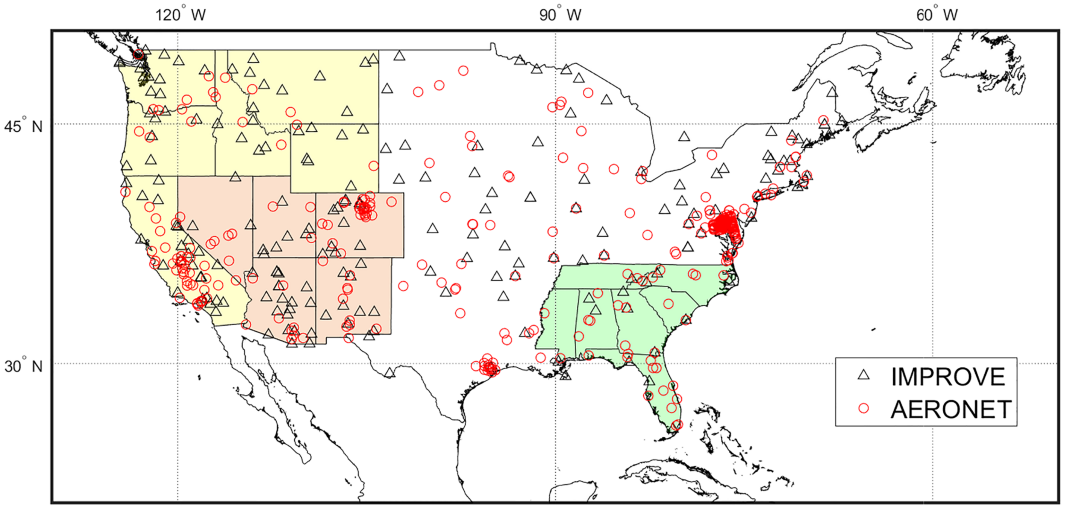

Figure 1. Pacific West (PW, yellow shading), southwest (SW, orange shading), and southeast (SE, green shading) with locations of AERONET and IMPROVE sites used in the study.

$$AAOD_{\mathrm{smoke},i} = \overline{AAOD_{\mathrm{smokyday},i}} - \overline{AAOD_{\mathrm{nonsmokyday},i}},\ i = 440, 675, 870, \text{and } 1,020 \text{ nm} \quad (7)$$

$$EAE_{\mathrm{smoke}} = -\frac{\ln\left(AOD_{\mathrm{smoke,440nm}}\right) - \ln\left(AOD_{\mathrm{smoke,1020nm}}\right)}{\ln(440) - \ln(1020)} \quad (8)$$

$$AAE_{\mathrm{smoke}} = -\frac{\ln\left(AAOD_{\mathrm{smoke,440nm}}\right) - \ln\left(AAOD_{\mathrm{smoke,1020nm}}\right)}{\ln(440) - \ln(1020)} \quad (9)$$

$$SSA_{\mathrm{smoke}} = \frac{\overline{AOD_{\mathrm{smokyday}}} \times \overline{SSA_{smokyday}} - \overline{\mathrm{AOD}_{\mathrm{nonsmokyday}}} \times \overline{SSA_{\mathrm{nonsmokyday}}}}{\overline{AOD_{\mathrm{smoke}}}} \quad (10)$$

where $\overline{species_{\mathrm{smokyday}}}$ and $\overline{species_{\mathrm{nonsmokyday}}}$ are mean concentrations of chemical species of interest on the smoky days and nonsmoky days, $\overline{AOD_{\mathrm{smokyday}}}$ and $\overline{SSA_{\mathrm{smokyday}}}$ are mean AOD and SSA on the smoky days in one region, and $\overline{AOD_{\mathrm{nonsmokyday}}}$ and $\overline{SSA_{\mathrm{nonsmokyday}}}$ are mean AOD and SSA on the nonsmoky days in the same region. We note that this method of isolating smoke properties from aerosol mixtures assumes that the nonsmoke properties are the same on smoky days and nonsmoky days, which is not necessarily true, and we discuss the potential implications of this assumption in the sections 3 and 4.

In order to estimate the uncertainty in our mean smoke properties, we deploy a bootstrap sampling method (Efron, 1979) to estimate the uncertainties of the mean values on the smoky and nonsmoky days for all the parameters used as inputs to equations (5)–(10) (chemical concentration, AOD, AAOD, and SSA) by resampling the data points after replacing the values of some points with duplicate values of other data points. We use the Matlab function "bootstrp" (https://www.mathworks.com/help/stats/bootstrp.html) to retrieve the uncertainty in the mean values by resampling the data sets 5,000 times each.

3. Results and Discussion

3.1. Surface Smoke Chemical Composition

Figure 2 shows the IMPROVE PM concentrations and composition on smoky (including both the smoke and nonsmoke contributions) and nonsmoky days. Smoke particles are mainly comprised of carbonaceous species, EC and OC (Levin et al., 2010; May et al., 2014). KNON is an important chemical marker emitted from biomass burning (Lee et al., 2010; Sullivan et al., 2008; Sullivan et al., 2019). As expected, all three species are enhanced on smoky days relative to nonsmoky days in all three regions (Figure 2), and the filter-based absorption is also enhanced in all three regions on smoky days (Figure S1 in the supporting information). All the species in the three regions are statistically significantly different (at the 0.05 level) on smoky and nonsmoky days, except KNON, Si, and coarse particles in the SW region (determined by running two-sample tests using the Matlab function ttest2). The absolute enhancement in these three species is most notable in the PW due to higher $PM_{2.5}$ concentrations on smoky days.

We also find that nitrate and sulfate concentrations are increased on smoky days. Souri et al. (2017) showed that biomass burning emitted negligible particulate nitrate but considerable amounts of gaseous precursors (NO_x). Their work demonstrated that the formation of aerosol-phase nitrate particles was mainly from the conversion of NO_x. Sulfate is enhanced more in the SE on smoky days relative to the other regions. While sulfate is not a typical tracer for biomass burning, both lab and field work have shown sulfate fractions were around 10–20% in smoke from the combustion of certain types of southeastern fuels (Kondo et al., 2011; Levin et al., 2010; May et al., 2014). Kondo et al. (2011) noted that sulfate deposited on SE vegetation can be released back into the atmosphere when the vegetation is burned.

Silicon and coarse particles (PM_{10}–$PM_{2.5}$ in Figure 2) are also enhanced on smoky days in all three regions, but this enhancement is strongest in the arid and semiarid SW. Silicon is a tracer for dust (Malm et al., 1994), and most dust mass resides in the coarse mode. Previous studies have suggested that fires in this region may loft dust from the surface in strong fire-driven updrafts (Lindsey et al., 2010; Peterson et al., 2018), and the SW is a dust-prone region even in the absence of lofting by fires (Hand et al., 2017). However, the environmental conditions that are favorable for fire (dry and fast surface winds) are also favorable for dust lofting, so we cannot rule out that the dust enhancement on smoky days may simply be due to correlation rather than causation.

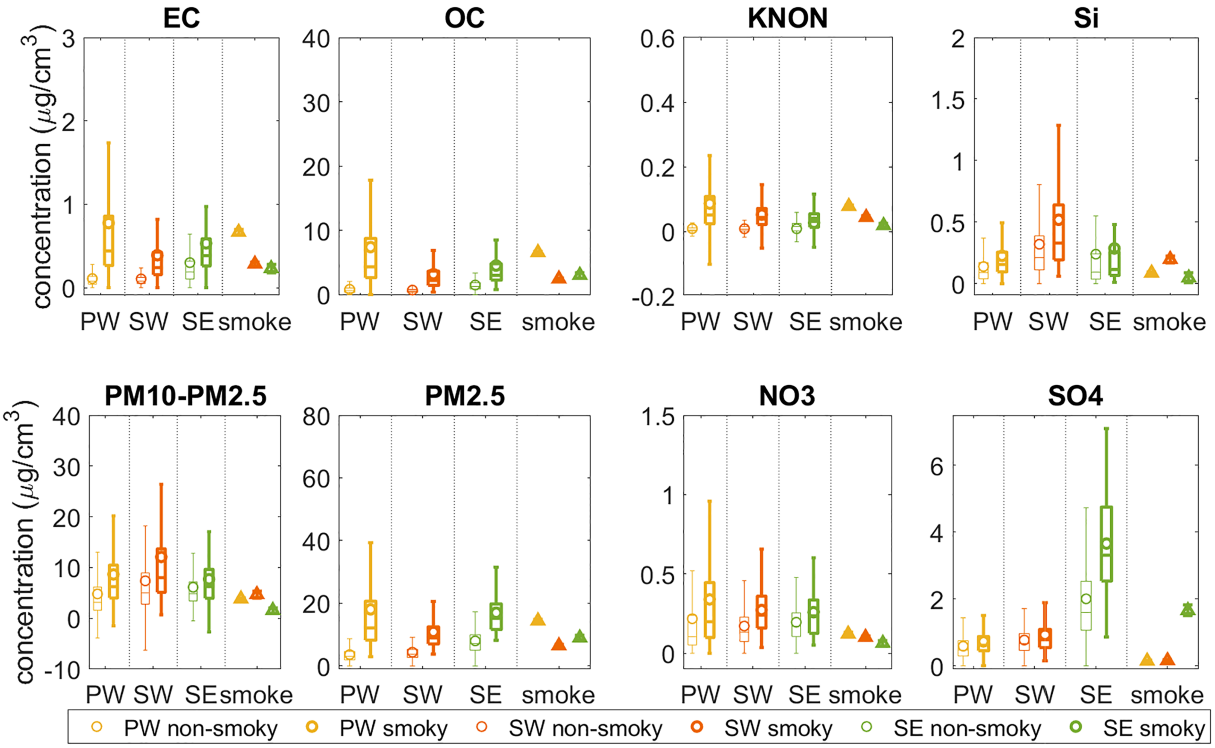

Figure 2. Box plots of EC, OC, nonsoil K (KNON), Si, coarse particles (PM_{10}–$PM_{2.5}$), $PM_{2.5}$, NO_3^-, and SO_4^{2-} (μg/m^3) for PW (yellow), SW (orange), and SE (green) United States for smoky and nonsmoky days and isolating the contributions of smoke itself for the three regions. The lines represent the median values, the boxes represent the interquartile and the whiskers correspond to approximately 99.3% coverage; the circles represent the average values. The mean smoke concentration (triangles) on smoky days is estimated by the mean difference between smoky and nonsmoky days using the bootstrap sampling method, and the error bars represent 1 standard deviation in the mean estimate found through the bootstrap method.

Figure 3 shows the fractional composition of smoke-specific $PM_{2.5}$ for each of the three regions. OM is the dominant species in smoke $PM_{2.5}$ across all regions, accounting for 68% in the PW, 57% in the SW, and 48% in the SE regions, the range of which is consistent with lab and field studies (Levin et al., 2010; May et al., 2014). A higher fraction of organics is expected to be emitted from smoldering burns while less organics are expected from flaming burns. However, the burned fuel types, burn area, and the distance from the fire location can also influence the organic loading due to the complex physical and chemical transformations (e.g., evaporation of organic aerosol as the plume dilutes and secondary aerosol formation) that can occur during transport of the smoke plume to the receptor sites. Thus, the difference in the OM fraction may not be attributed to one single reason.

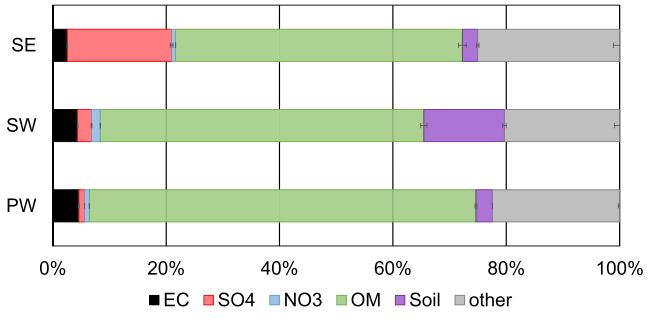

Figure 3. Mean smoke $PM_{2.5}$ fractional composition for the PW, SW, and SE regions. Smoke $PM_{2.5}$ mass and species mass concentrations are calculated by the mean difference between smoky and nonsmoky days. The "other" fraction is calculated by [$PM_{2.5}$] − [EC] − [SO4] − [NO3] − [OM] − [Soil]. The error bars represent the standard deviation for mean estimate in the bootstrap calculation.

A lower fraction of EC is emitted during the smoldering phase compared to the flaming phase (Jen et al., 2019; McMeeking et al., 2009); thus, we might expect different fractions of EC in the different regions based on the dominant fire types. Indeed, our results do show that the EC fraction is 4.8% in the PW and 4.5% in the SW, compared to 2.3% in the SE. There are also higher KNON fractions observed in the PW (0.55%, not included in Figure 3) and SW (0.56%) compared to the SE (0.17%). This difference in KNON fractions also indicates that fires in the western regions are more flaming than in the SE, as flaming fires release more KNON than smoldering fires (Lee et al., 2010; Sullivan et al., 2019). Chen et al. (2010) showed the release of NO_x was also related to combustion condition, with more NO_x from the flaming phase and more NH_3 from the smoldering phase. This may also explain a greater enhancement of nitrate in the western regions (1.1% in the PW and 1.6% in the SW), where flaming fires may dominate, compared to the SE (0.69%).

Other notable differences in the smoke aerosol composition between the two western regions and the SE are the sulfate and soil fractions. The sulfate fraction is 18% in the SE and only 1–3% in the two western regions, which may be due to fuel differences, as discussed earlier. The soil fraction is 16% in the SW and only 2.6% and 4.0% in the PW and SW, consistent with the discussion above about SW dust enhancements on smoky days. The "Other" category contributes 22% and 19% to the normalized smoky day $PM_{2.5}$ in the two western regions and around 27% in the SE. Levin et al. (2010) showed that the emissions from SE fuels have significant inorganic fractions (e.g., NH_4Cl, $(NH_4)_2SO_4$, KCl). However, the IMPROVE network does not measure NH_4^+; thus, the "Other" category may partially represent inorganic species not explicitly measured.

Schlosser et al. (2017) also found the concentrations of nitrate, fine soil, and coarse particles increased on peak EC days, that is, their defined smoke-impact days in the western United States from 2005 and 2015, consistent with our results. But their results showed that the percentage of fine soil and coarse mass increased more in Oregon and Washington due to lower background concentrations on nonfire days. This is different from our results, that show that the dust concentration in smoke is highest in the SW, probably due to our different approaches in selecting smoke-impacted days. Schlosser et al. (2017) determined smoke-impacted days as days with high EC (mean + 2σ for the 10-week period centered around this day), while our method uses the overlap with HMS and further restricts "smoky days" to the subset with high $PM_{2.5}$ loadings (> mean + σ for our selected April–September time frame).

Smoke from one of our defined regions can impact one or more of the other regions, and smoke from outside any of these regions can also be transported into the United States (e.g., Gebhart et al., 2001; Kreidenweis et al., 2001; Mathur, 2008). For example, from the HMS product, we observed some cases for which smoke plumes from Canada extended into the NW, SW, and even the SE regions; however, smoke from Canadian fires most often impacts the central and northeastern United States, regions not considered in our analyses (Brey, Barnes, et al., 2018). As well, in the springtime, smoke plumes from Central America can be transported to the SE region, as reported in the studies of Park et al. (2003) and Wang et al. (2006, 2009). Brey, Ruminski, et al. (2018) combined the HMS product and HYSPLIT forward trajectory data to connect summertime (June–September) smoke plumes to their sources (see their Figure 13). They found that in the NW, SW, and SE, smoke hours were contributed mainly by fires within these regions, although smoke was exchanged to a significant extent among western regions. Based on these considerations and for our April-September time period, we expect the properties of smoke in our western regions to be largely from fires within the western regions, but in the southeast, we expect a mixture of smoke produced by fires in the southeast and long-range-transported smoke from Central American or, occasionally, Canadian fires.

It is noted that in 2011, the IMPROVE network shifted to a $PAN_{analytical}$ XRF system that performs the elemental analysis (Hand et al., 2019), and an increase at the same time in the relative humidity condition in the laboratory may also have influenced the gravimetric measurements. To test the influences of these 2011 protocol changes on our results, we compared the data for the two groupings, 2008–2010 and 2011–2017, in Figures S2 and S3. The main conclusions from our work regarding smoke differences between regions remain unchanged due to the change in analysis techniques in 2011.

As it is assumed that high TC concentrations are associated with the presence of smoke, Figures S4 and S5 show the box plots of chemical species of interest and the $PM_{2.5}$ chemical composition for isolated smoke using the TC criterion (TC > mean + 1 standard deviation). Our overall conclusions regarding major $PM_{2.5}$ compositional differences in smoke between these three regions are mostly not affected by applying this alternative criterion for identifying smoke impacts at the surface, namely, the SW has the highest fraction of soil and the SE has the highest fraction of sulfate. Although the SE still has the lowest fraction of EC, the alternative TC criterion reduces the differences between this region and the western regions due to removing some dust influenced days from the "smoky day" category (although these days may have been smoke impacted).

3.2. Columnar Smoke Optical Properties

We use the AERONET data to examine the optical properties of smoke aerosol in the different regions. Unsurprisingly, AOD, and AAOD are higher on smoky days than nonmoky days in all regions (Figures S6

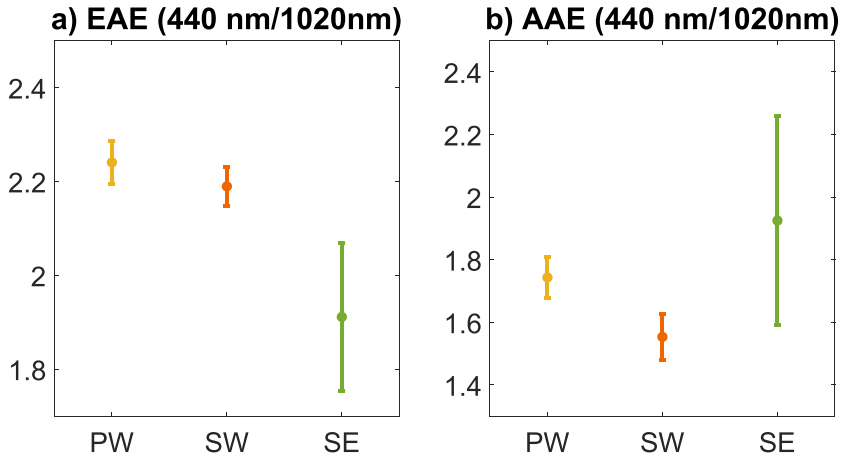

Figure 4. Smoke (a) Extinction Ångström Exponent (EAE, 440/1,020 nm) and (b) Absorption Ångström Exponent (AAE, 440/1,020 nm) in the PW, SW, and SE regions. The whiskers represent 1 standard deviation in the estimate of our mean smoke Ångström Exponent based on the bootstrap sampling estimation.

and S7), similar to the surface $PM_{2.5}$ and EC concentrations on the smoky days shown in the section above. For the rest of this section, we focus more on the intensive smoke properties derived from the AERONET data (with the exception of the refractive index, where we focus on smoky versus nonsmoky days due to the challenge of isolating the smoke refractive index).

3.2.1. EAE and AAE

The Ångström exponent is an intensive property describing the spectral dependence of optical properties such as extinction or absorption. EAE is related mostly to particle size (Schuster et al., 2006) and AAE is influenced by both particle size and chemical composition (Liu et al., 2018; Russell et al., 2010). EAE and AAE are both statistically different (p values all < 0.05) between smoky and nonsmoky days, with higher values on smoky days than nonsmoky days in all regions (Figures S8a and S8b), suggesting changes in both particle size and chemical composition. Figure 4 shows the mean EAE and AAE values that we isolated for smoke using equations (8) and (9) for the 440 and 1,020 nm wavelength pair (EAE_{smoke} and AAE_{smoke}). EAE_{smoke} is largely similar between the three regions (2.24, 2.19, and 1.91 in the PW, SW, and SE, respectively), considering that EAE values calculated from AAE and SSA reported in the Fourth Fire Lab at Missoula Experiment (FLAME-4, Pokhrel et al., 2016) laboratory measurements ranged from 0.84 to 4.05. Our AAE_{smoke} is 1.74, 1.55, and 1.89 in the PW, SW, and SE, respectively. AAE measured in the Fire Laboratory at Missoula Experiment 3 (FLAME-3) ranged from 1.74–6.98 (McMeeking et al., 2014), while measurements from FLAME-4 had a wider range of values across burns (0.85–4 for most fuels, with peat and chamise burning ranging from 4–10; Pokhrel et al., 2016). Our AAE values also show less variation compared with laboratory measurements. These differences may suggest that our results determined using ambient smoke plumes are more representative of smoke from the burning of several types of vegetation and of smoke that has been processed over time, as compared to fresh smoke sampled in the laboratory studies. We also calculate AAE_{smoke} for 440/675 nm, 675/870 nm, and 870/1,020 nm for the three regions in Table S1. AAE_{smoke} increases from shorter wavelength pairs to longer wavelength pairs in each region, showing a trend in AAE similar to the trend reported for tar brown carbon in Corbin et al. (2019).

3.2.2. Volume Size Distributions

Figure 5 shows our estimates for the normalized smoke size distribution for each region using the differences between the mean volume size distributions for smoky and nonsmoky days, normalizing each size bin by the total volume concentration (Figure S9 shows the average volume size distributions on the smoky and nonsmoky days in the three regions that are used to create Figure 5). The SE has larger fine-mode particles (volume mode diameter is 0.39 μm), than the PW and SW (volume mode diameter: 0.30 μm both regions). All three regions have the same mode diameter for the coarse particles (10.12 μm). The SE has more fine-particle volume in the normalized distribution compared with the PW and SW regions, while the SW has the most coarse-particle volume. A potential reason for the differences in the size distribution may be different combustion behaviors, that is, more flaming in the PW and SW and more smoldering in the SE, as might

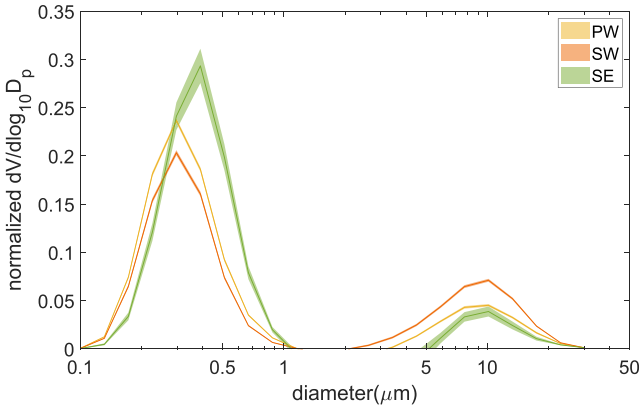

Figure 5. Normalized smoke volume size distribution (i.e., difference of the mean volume size distribution between smoky and nonsmoky days normalized to each have an area under the curve of (1) in the PW, SW, and SE regions. The shading represents 1 standard deviation in the estimate of our mean smoke distributions based on the bootstrap sampling estimation.

be associated with prescribed burning. The flaming phase of burning usually produces smaller particles while the smoldering phase generates larger particles (Reid, Koppmann, et al., 2005); however, coagulation, condensation, and evaporation in the plumes can also significantly modify the size distribution during aging (Hodshire et al., 2019). Another potential reason for larger fine-mode particles in the SE is differences in hygroscopic particle growth between regions. RH is often higher in the SE (e.g., 72.9 ± 8.1% (1 σ) from April to September 2017 from NOAA USCRN/USRCRN product) compared to the two western regions (e.g., 56.4 ± 15.2% in the PW and 43.3 ± 14.6% in the SW in the same period, Figure S10). Because there is a higher fraction of sulfate in the smoke aerosol in the SE compared to the PW and SW (Figure 3), in addition to the higher RH in the SE, the aerosol in the SE likely contains more water, growing the fine smoke particles to larger diameters. Finally, the difference in coarse particles may be related to environmental conditions (i.e., dust emissions in the SW) mentioned previously.

3.2.3. Refractive Index

The refractive index reflects the chemical composition of particles, including the possible water content of the aerosol; and it determines (along with size and shape) the particle scattering and absorption. Table 2 and Figure S11 show the refractive indices on smoky and nonsmoky days in the three regions. These refractive indices are calculated across all aerosol sizes in the AERONET inversion. Refractive indices are similar between the PW and the SW regions on nonsmoky ($1.52 + 0.0095i$ in the PW and $1.53 + 0.016i$ in the SW) and smoky days ($1.52 + 0.0072i$ in PW and $1.53 + 0.010i$ in the SW). However, both the real and imaginary parts are lower in the SE ($1.49 + 0.0081i$ in the nonsmoky days and $1.48 + 0.0067i$ in the smoky days) compared to the PW and SW regions. As discussed in the previous subsection, the SE smoke may contain more water than the other regions due to higher RH and a higher sulfate fraction. The refractive index for water is $1.33 + 0.0i$, which is lower than most other aerosol species. Based on the volume mixing rule for estimating the refractive index, additional water will lower both parts of the refractive index. The real parts of the refractive index are similar for smoky and nonsmoky days for all three regions, while the imaginary parts show a slight decrease on smoky days (Figure S11), which may be due to a decrease in the relative contribution of dust to aerosol volume on smoky days (discussed further in the next subsection).

3.2.4. SSA

SSA is the ratio of scattering to extinction. Dubovik et al. (2000) and Andrews et al. (2017) showed that the uncertainty in derived SSA is 0.03 for AOD ≥ 0.2 and increases to 0.06 for AOD < 0.2. To estimate the total uncertainty in SSA at each wavelength from the varying uncertainties in the underlying data set, we incorporated these SSA uncertainties in a bootstrap estimate assuming that SSA uncertainty is independent between data points. Figure 6a shows the mean SSA on smoky and nonsmoky days and the uncertainties in the mean SSA, while Figure 6b shows the mean SSA_{smoke} and the estimated uncertainties, for the three regions at four wavelengths. We found that the SSA (440 nm) on nonsmoky days was lowest in the SW (0.89) compared to the PW (0.93) and SE (0.94). Figure S12 shows that the SW has both the highest Si fractions (indicator for dust influence) and the lowest SSA; hence, we hypothesize that dust drives the regional variability of SSA on nonsmoky days. The SSA in the SE is the highest, which again may be due to the higher RH (Figure S10) and higher sulfate concentrations (Figure S13), which could increase aerosol water, and hence, cause more scattering relative to absorption.

For smoky days, the SSA (440 nm) is 0.94 in the PW, 0.93 in the SW, and 0.95 in the SE. These smoky-day values are statistically different from the respective nonsmoky values in the regions and the smoke SSAs in the different regions are statistically different from each other, according to two-sample *t* tests (*p* values all < 0.0001). Nikonovas et al. (2015) showed that

Table 2
Mean Refractive Index for the PW, SW, and SE regions.

		PW	SW	SE
Nonsmoky	440 nm	$1.52 + 0.011i$	$1.53 + 0.020i$	$1.50 + 0.0081i$
	675 nm	$1.52 + 0.0095i$	$1.53 + 0.016i$	$1.49 + 0.0081i$
	870 nm	$1.52 + 0.012i$	$1.53 + 0.018i$	$1.49 + 0.0094i$
	1,020 nm	$1.52 + 0.013i$	$1.52 + 0.019i$	$1.48 + 0.010i$
Smoky	440 nm	$1.52 + 0.0082i$	$1.53 + 0.012i$	$1.49 + 0.0068i$
	675 nm	$1.52 + 0.0072i$	$1.53 + 0.010i$	$1.48 + 0.0067i$
	870 nm	$1.52 + 0.0077i$	$1.53 + 0.011i$	$1.48 + 0.0071i$
	1,020 nm	$1.52 + 0.0078i$	$1.52 + 0.012i$	$1.48 + 0.0073i$

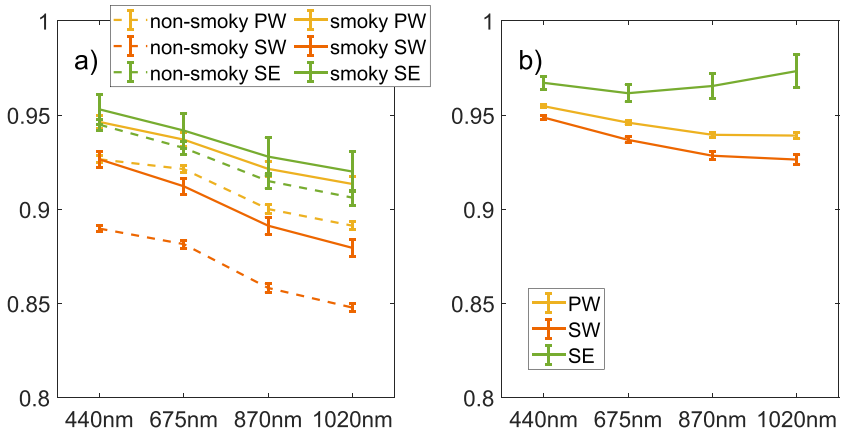

Figure 6. (a) Mean single scattering albedo (SSA) for 440, 675, 870, and 1020 nm for nonsmoky and smoky days in the three regions, as derived from AERONET data from 2008 to 2017; (b) derived mean smoke SSA for the PW, SW, and SE regions; the error bars represent 1 standard deviation in the estimate of the mean smoke SSA, using the bootstrap method.

the smoke-influenced AERONET SSA for fires from the northern boreal and temperate forests in North America and Eurasia was about 0.943–0.949, which is similar to our study. Shi, Cheng, et al. *(*2019*)* showed that the smoke-influenced AERONET SSA (440 nm) was 0.952 for forest and peat, 0.849 for grass and shrub, and 0.873 for a mixture of the two fuels. Our results for all three regions fall between their "forest and peat" and "grass and shrub" type values, and as our values are an average of smoke over a decade and over broad regions, it is likely that there are a variety of fuel types burned.

In all three regions, SSA is higher on smoky days compared to nonsmoky days. This SSA difference may be attributed to an increase in fine-mode fraction and/or a decrease in the imaginary part of the refractive index, as mentioned in section 3.2.3 (Figure 6a). A decrease in the imaginary part of the refractive index can be attributed to a change in the chemical composition of the aerosol (including water content), while an increase in the fine mode is related to a change in the normalized particle size distribution (Figure S9). We hypothesize that the higher SSA on smoky versus nonsmoky days is due to dust contributing to a higher fraction of extinction on nonsmoky days. The addition of smoke, with a higher SSA than dust, would increase the overall SSA observed by AERONET. Figures 2, S9, and S14 show that the fine mode is a higher fraction of the total fine + coarse mass, volume, and AOD on smoky days compared to nonsmoky days, which supports this hypothesis.

Figure 6b shows the smoke SSA (SSA_{smoke}) estimated from equation (10) in the three regions. SSA_{smoke} (440 nm) is 0.95 ± 0.001 in the PW and SW regions and 0.97 ± 0.004 in the SE (Figure 6b). The standard deviation is calculated from the bootstrap estimate, with consideration of the uncertainty in SSA reported for the AERONET data (Andrews et al., 2017*;* Dubovik et al., 2000). Our method cannot determine the plume age, but the values are consistent with the AERONET data being primarily for aged smoke (Pokhrel et al., 2016; Vakkari et al., 2014). The smoke SSA from wildfires in the Yucatan (Yokelson et al., 2009) increased from 0.75 to 0.9 as the smoke plume aged in the first 1.4 hr, which implies that our observed smoke is aged on average. The plot of AAE_{smoke} versus SSA_{smoke} (Figure S15) shows that AERONET smoke data for the three regions deviated from the laboratory measurements in FLAME 3 and FLAME-4, with lower AAE and high SSA, also indicating our observed smoke is aged smoke relative to the fresh smoke measured in the laboratory experiments.

SSA_{smoke} is higher in the SE than the two western regions at all wavelengths. This result is consistent with the EC fraction of (dry) $PM_{2.5}$ in SE smoke being half of that of the western regions (Figure 3). More prescribed and/or smoldering fires may partially explain the higher SSA values in the SE compared with a more frequent occurrence of large flaming wildfires in the PW and SW regions. As discussed above, long-range-transported smoke from Central America can also impact the SE region. This long-range-transported smoke was shown in earlier studies to have higher SSA than fresher smoke (Kreidenweis et al., 2001; Wang et al.,

2006). In addition, the SE has higher RH and a larger sulfate fraction in the smoke, which increases aerosol water content and thus, contributes to the higher SSA.

To test the robustness of our derived SSA_{smoke}, we also calculate the SSA_{smoke} using a subset of the smoke days when the fine-mode AOD is larger than 0.3 (when smoke is likely the dominant contributor to AOD, Figure S16). SSA_{smoke} (440 nm, AOD > 0.3) is 0.96 in the two western regions and 0.98 in the SE. These values are slightly higher than the SSA_{smoke} (440 nm) calculated using all the data points, but the SSA_{smoke} in the SE is still higher than the two western regions. Therefore, using a subset of data generates a similar result for smoke SSA for the three regions, mainly that smoke in the SE has a higher SSA while the PW and SW have very similar SSA values.

4. Discussion and Conclusions

Each region studied here has unique smoke compositional characteristics: the SW smoke has the highest fraction of soil but is similar in other respects—particularly in the fractional contribution of BC—to PW smoke, whereas the SE smoke has a high fractional contribution of sulfate but a soil fraction similar to that of PW smoke. These chemical characteristics are manifested in the derived smoke aerosol optical properties, in particular, the SE smoke has the highest SSA, consistent with the lowest fractional contributions of BC. The burning environment may play a significant role in the different SSA values. The SE is more humid, and the smoke has a higher sulfate (strongly hygroscopic) fraction relative to the two western regions. Thus, smoke in the SE likely contains more water, which increases the SSA. While it is generally assumed that black carbon emitted from biomass burning decreases ambient SSA relative to nonsmoke aerosol, we find that the SSA on smoky days was higher than on non-smoky days, on average, for all three regions. This increased SSA on smoky days may be due to a change in chemical composition (the fraction of mass from dust is lower on smoky days) and potentially a change in particle size (increased contributions of the fine mode) on smoky days.

Fires in the arid and semiarid SW produce smoke with the lowest-SSA particles, consistent with our analysis that shows that there is more dust mixed into the smoke. However, the spectral dependencies of SSA for PW and SW smoke are remarkably similar, despite the differences in composition, as are the EAE and AAE. Thus, smoke in these regions might be well represented by a single "western US" smoke optical model. This result may be largely attributed to the similar PW and SW volume distributions as derived from optical measurements, although the fractional volume in the coarse mode is somewhat higher for the SW, consistent with the stronger contributions from soil. However, these differences in both chemical composition and volume distributions do not manifest in strong mean regional differences in optical properties between smoke in the PW and SW, for the wavelengths considered here. In contrast, the SE smoke mean volume distribution has a much higher fractional volume in the fine mode, and the mean fine-mode particle size is larger than for PW and SW smoke. Thus, it appears that a different optical model may be needed to best represent SE smoke in radiative transfer models.

While we attribute most of the differences in the smoke chemical and optical properties between regions to different environmental conditions and fire types, the age of the smoke plume could also alter these properties. Thus, one limitation to our study is that we cannot differentiate between (relatively) fresh and aged plumes using the HMS product. We did attempt a cursory look at this by calculating the size and number of HMS smoke polygons (plumes) at each AERONET site (Figure S17). All three regions experienced a range in sizes of smoke plumes, suggesting that these differences are not simply due to differences between small prescribed fires in the SE and large wildfires in the PW. However, due to the prevailing transport pattern over the United States (Brey, Ruminski, et al., 2018), the large plumes in the PW were more likely due to (relatively) local fires. Smoke plumes from these western fires can be transported very long distances out of our designated regions; thus, the sites in the SE can experience aged smoke emitted from the western regions mixed with fresh smoke from local fires in the same period (Brey, Ruminski, et al., 2018). Further, the SE can also be impacted during the springtime by aged smoke from Mexico and Central America. Thus, in our analyses, the smoke properties in the PW and SW may represent relatively fresh smoke (though much of the smoke may still be over a day old before leaving the region) while the SE smoke may include both "fresh" and aged, long-range-transported smoke. As can be seen in Figures 4 and 6, the data for the SE had considerably more variability than in the other

regions, which may represent such varied influences. More research is needed to develop methodologies to separate observations based on source regions and age, and to understand how plume age may impact smoke properties in these different regions.

An additional limitation of the study is that when isolating the properties of smoke aerosol, we assume that the mean nonsmoke properties are the same on smoky days as they are on nonsmoky days, from which the mean smoke properties are estimated. Because wildfires tend to occur more often during periods of high temperatures, low precipitation, and fast winds, the nonsmoke properties on smoky days may not be the same as on nonsmoky days due to this bias of fire occurrence toward certain meteorological conditions. It is possible that the increased coarse/dust aerosol that we observe to be associated with smoke, relative to background days, may be because dust emissions are also favorable during periods of high temperatures, low precipitation, and fast winds.

Landscape fires are an increasingly important source of particulate matter in the United States and other parts of the world, making it necessary to better quantify smoke impacts. The derived landscape-fire smoke aerosol composition, size, and optical properties in this paper can be used to improve satellite retrievals of aerosol loadings during smoke events by considering regional differences in smoke properties, to evaluate smoke aerosol properties in air quality and climate models, and to improve estimates of the impacts of smoke on the Earth's radiative budget.

Acknowledgments
This work is supported by the U.S. NOAA, an Office of Science, Office of Atmospheric Chemistry, Carbon Cycle, and Climate Program, under the cooperative agreement award NA17OAR430001; the U.S. NSF Atmospheric Chemistry program, under Grant AGS-1559607; the Joint Fire Science Program under project 14-1-03-26; and the Office of Naval Research under Award N00014-16-1-2040. IMPROVE is a collaborative association of state, tribal, and federal agencies and international partners. U. S. Environmental Protection Agency is the primary funding source, with contracting and research support from the National Park Service. The Air Quality Group at the University of California, Davis is the central analytical laboratory, with ion analysis provided by Research Triangle Institute, and carbon analysis provided by Desert Research Institute. We thank the principal investigators and their staff for establishing and maintaining the AERONET sites (https://aeronet.gsfc.nasa.gov/) used in this investigation.

References

Abram, N. J., Gagan, M. K., McCulloch, M. T., Chappell, J., & Hantoro, W. S. (2003). Coral reef death during the 1997 Indian Ocean dipole linked to Indonesian wildfires. *Science*, *301*(5635), 952–955. https://doi.org/10.1126/science.1083841

Andrews, E., Ogren, J. A., Kinne, S., & Samset, B. (2017). Comparison of AOD, AAOD and column single scattering albedo from AERONET retrievals and in situ profiling measurements. *Atmospheric Chemistry and Physics*, *17*, 6041–6072. https://doi.org/10.5194/acp-17-6041-2017

Bond, T. C., Doherty, S. J., Fahey, D. W., Forster, P. M., Berntsen, T., DeAngelo, B. J., et al. (2013). Bounding the role of black carbon in the climate system: A scientific assessment. *Journal of Geophysical Research: Atmospheres*, *118*, 5380–5552. https://doi.org/10.1002/jgrd.50171

Brewer, P., & Moore, T. (2009). Source contributions to visibility impairment in the southeastern and western United States. *Journal of the Air & Waste Management Association*, *59*(9), 1070–1081. https://doi.org/10.3155/1047-3289.59.9.1070

Brey, S. J., Barnes, E. A., Pierce, J. R., Wiedinmyer, C., & Fischer, E. V. (2018). Environmental conditions, ignition type, and air quality impacts of wildfires in the southeastern and western United States. *Earth's Future*, *6*(10), 1442–1456. https://doi.org/10.1029/2018EF000972

Brey, S. J., Ruminski, M., Atwood, S. A., & Fischer, E. V. (2018). Connecting smoke plumes to sources using hazard mapping system (HMS) smoke and fire location data over North America. *Atmospheric Chemistry and Physics*, *18*(3), 1745–1761.

Burling, I. R., Yokelson, R. J., Griffith, D. W. T., Johnson, T. J., Veres, P., Roberts, J. M., et al. (2010). Laboratory measurements of trace gas emissions from biomass burning of fuel types from the southeastern and southwestern United States. *Atmospheric Chemistry and Physics*, *10*(22), 11,115–11,130. https://doi.org/10.5194/acp-10-11115-2010

Cascio, W. E. (2018). Wildland fire smoke and human health. *Science of the Total Environment*, *624*, 586–595. https://doi.org/10.1016/j.scitotenv.2017.12.086

Chen, L.-W. A., Verburg, P., Shackelford, A., Zhu, D., Susfalk, R., Chow, J. C., & Watson, J. G. (2010). Moisture effects on carbon and nitrogen emission from burning of wildland biomass. *Atmospheric Chemistry and Physics*, *10*(14), 6617–6625. https://doi.org/10.5194/acp-10-6617-2010

Collier, S., Zhou, S., Onasch, T. B., Jaffe, D. A., Kleinman, L., Sedlacek, A. J. III, et al. (2016). Regional influence of aerosol emissions from wildfires driven by combustion efficiency: Insights from the BBOP campaign. *Environmental Science & Technology*, *50*(16), 8613–8622. https://doi.org/10.1021/acs.est.6b01617

Corbin, J. C., Czech, H., Massabò, D., de Mongeot, F. B., Jakobi, G., Liu, F., et al. (2019). Infrared-absorbing carbonaceous tar can dominate light absorption by marine-engine exhaust. *npj Climate and Atmospheric Science*, *2*(1), 12. https://doi.org/10.1038/s41612-019-0069-5

Crouse, D. L., Peters, P. A., van Donkelaar, A., Goldberg, M. S., Villeneuve, P. J., Brion, O., et al. (2012). Risk of nonaccidental and cardiovascular mortality in relation to long-term exposure to low concentrations of fine particulate matter, a Canadian national-level cohort study. *Environmental Health Perspectives*, *120*(5), 708–714. https://doi.org/10.1289/ehp.1104049

de Graaf, M., Tilstra, L. G., Wang, P., & Stammes, P. (2012). Retrieval of the aerosol direct radiative effect over clouds from spaceborne spectrometry. *Journal of Geophysical Research*, *117*, D07207. https://doi.org/10.1029/2011JD017160

Dennison, P. E., Brewer, S. C., Arnold, J. D., & Moritz, M. A. (2014). Large wildfire trends in the western United States, 1984—2011. *Geophysical Research Letters*, *41*, 2928–2933. https://doi.org/10.1002/2014GL059576

Dubovik, O., Holben, B., Eck, T. F., Smirnov, A., Kaufman, Y. J., King, M. D., et al. (2002). Variability of absorption and optical properties of key aerosol types observed in worldwide locations. *Journal of the Atmospheric Sciences*, *59*(3), 590–608. https://doi.org/10.1175/1520-0469(2002)059<0590:VOAAOP>2.0.CO;2

Dubovik, O., Smirnov, A., Holben, B. N., King, M. D., Kaufman, Y. J., Eck, T. F., & Slutsker, I. (2000). Accuracy assessment of aerosol optical properties retrieval from AERONET sun and sky radiance measurements. *Journal of Geophysical Research*, *105*, 9791–9806. https://doi.org/10.1029/2000JD900040

Eck, T. F., Holben, B. N., Reid, J. S., Sinyuk, A., Hyer, E. J., O'Neill, N. T., et al. (2009). Optical properties of boreal region biomass burning aerosols in central Alaska and seasonal variation of aerosol optical depth at an Arctic coastal site. *Journal of Geophysical Research*, *114*, D11201. https://doi.org/10.1029/2008JD010870

Efron, B. (1979). Bootstrap methods: Another look at the jackknife. *The Annals of Statistics*, *7*, 1–26.

Ford, B., Val Martin, M., Zelasky, S. E., Fischer, E. V., Anenberg, S. C., Heald, C. L., & Pierce, J. R. (2018). Future fire impacts on smoke concentrations, visibility, and health in the contiguous United States. *GeoHealth*, *2*, 229–247. https://doi.org/10.1029/2018GH000144

Gan, R. W., Ford, B., Lassman, W., Pfister, G., Vaidyanathan, A., Fischer, E., et al. (2017). A comparison of smoke estimation methods and their association with wildfire smoke and cardiopulmonary-related hospital admissions during the 2012 Washington wildfires. *GeoHealth*, *1*, 122–136. https://doi.org/10.1002/2017GH000073

Gebhart, K. A., Kreidenweis, S. M., & Malm, W. C. (2001). Back-trajectory analyses of fine particulate matter measured at Big Bend National Park in the historical database and the 1996 scoping study. *Science of the Total Environment*, *276*(1-3), 185–204. https://doi.org/10.1016/S0048-9697(01)00779-3

Giles, D. M., Sinyuk, A., Sorokin, M. G., Schafer, J. S., Smirnov, A., Slutsker, I., et al. (2019). Advancements in the Aerosol Robotic Network (AERONET) version 3 database—Automated near-real-time quality control algorithm with improved cloud screening for Sun photometer aerosol optical depth (AOD) measurements. *Atmospheric Measurement Techniques*, *12*(1), 169–209. https://doi.org/10.5194/amt-12-169-2019

Hand, J. L., Gill, T. E., & Schichtel, B. A. (2017). Spatial and seasonal variability in fine mineral dust and coarse aerosol mass at remote sites across the United States. *Journal of Geophysical Research: Atmospheres*, *122*, 3080–3097. https://doi.org/10.1002/2016JD026290

Hand, J. L., Prenni, A. J., Schichtel, B. A., Malm, W. C., & Chow, J. C. (2019). Trends in remote PM2.5 residual mass across the United States: Implications for aerosol mass reconstruction in the IMPROVE network. *Atmospheric Environment*, *203*, 141–152. https://doi.org/10.1016/j.atmosenv.2019.01.049

Hodshire, A. L., Bian, Q., Ramnarine, E., Lonsdale, C. R., Alvarado, M. J., Kreidenweis, S. M., et al. (2019). More than emissions and chemistry: Fire size, dilution, and background aerosol also greatly influence near-field biomass burning aerosol aging. *Journal of Geophysical Research: Atmospheres*, *124*, 5589–5611. https://doi.org/10.1029/2018JD029674

Jen, C. N., Hatch, L. E., Selimovic, V., Yokelson, R. J., Weber, R., Fernandez, A. E., et al. (2019). Speciated and total emission factors of particulate organics from burning western US wildland fuels and their dependence on combustion efficiency. *Atmospheric Chemistry and Physics*, *19*(2), 1013–1026. https://doi.org/10.5194/acp-19-1013-2019

Johnston, F. H., Henderson, S. B., Chen, Y., Randerson, J. T., Marlier, M., DeFries, R. S., et al. (2012). Estimated global mortality attributable to smoke from landscape fires. *Environmental Health Perspectives*, *120*(5), 695–701. https://doi.org/10.1289/ehp.1104422

Kondo, Y., Matsui, H., Moteki, N., Sahu, L., Takegawa, N., Kajino, M., et al. (2011). Emissions of black carbon, organic, and inorganic aerosols from biomass burning in North America and Asia in 2008. *Journal of Geophysical Research*, *116*, D08204. https://doi.org/10.1029/2010JD015152

Kreidenweis, S. M., Petters, M. D., & DeMott, P. J. (2008). Single-parameter estimates of aerosol water content. *Environmental Research Letters*, *3*, 035002. https://doi.org/10.1088/1748-9326/3/3/035002

Kreidenweis, S. M., Remer, L. A., Bruintjes, R., & Dubovik, O. (2001). Smoke aerosol from biomass burning in Mexico: Hygroscopic smoke optical model. *Journal of Geophysical Research*, *106*(D5), 4831–4844. https://doi.org/10.1029/2000JD900488

Lee, T., Sullivan, A. P., Mack, L., Jimenez, J. L., Kreidenweis, S. M., Onasch, T. B., et al. (2010). Chemical smoke marker emissions during flaming and smoldering phases of laboratory open burning of wildland fuels. *Aerosol Research Letters*, *44*(9). https://doi.org/10.1080/02786826.2010.499884

Levin, E. J. T., McMeeking, G. R., Carrico, C. M., Mack, L. E., Kreidenweis, S. M., Wold, C. E., et al. (2010). Biomass burning smoke aerosol properties measured during Fire Laboratory at Missoula Experiments (FLAME). *Journal of Geophysical Research*, *115*, D18210. https://doi.org/10.1029/2009JD013601

Lindsey, D. T., Miller, S. D., & Grasso, L. (2010). The impacts of the 9 April 2009 dust and smoke on convection. *Bulletin of the American Meteorological Society*, *91*, 991–995.

Liu, C., Chung, C. E., Yin, Y., & Schnaiter, M. (2018). The absorption Ångström exponent of black carbon: From numerical aspects. *Atmospheric Chemistry and Physics*, *18*(9), 6259–6273. https://doi.org/10.5194/acp-18-6259-2018

Liu, J. C., Pereira, G., Uhl, S. A., Bravo, M. A., & Bell, M. L. (2015). A systematic review of the physical health impacts from non-occupational exposure to wildfire smoke. *Environmental Research*, *136*, 120–132. https://doi.org/10.1016/j.envres.2014.10.015

Loría-Salazar, S. M., Holmes, H. A., Arnott, W. P., Barnard, J. C., & Moosmüller, H. (2016). Evaluation of MODIS columnar aerosol retrievals using AERONET in semi-arid Nevada and California, U.S.A., during the summer of 2012. *Atmospheric Environment*, *144*, 345–360. https://doi.org/10.1016/j.atmosenv.2016.08.070

Malm, W. C., & Schichtel, B. A. (2013). Uncertainty associated with estimating a short-term (1-3 hr) particulate matter concentration from a human-sighted visual range, Dec, available at: https://www.firescience.gov/projects/13-C-01-01/project/13-C-01-01_final_report.pdf

Malm, W. C. J., Sisler, F., Huffman, D., Eldred, R. A., & Cahill, T. A. (1994). Spatial and seasonal trends in particle concentration and optical extinction in the United States. *Journal of Geophysical Research*, *99*(D1), 1347–1370.

Mathur, R. (2008). Estimating the impact of the 2004 Alaskan forest fires on episodic particulate matter pollution over the eastern United States through assimilation of satellite-derived aerosol optical depths in a regional air quality model. *Journal of Geophysical Research*, *113*, D17302. https://doi.org/10.1029/2007JD009767

May, A. A., McMeeking, G. R., Lee, T., Taylor, J. W., Craven, J. S., Burling, I., et al. (2014). Aerosol emissions from prescribed fires in the United States: A synthesis of laboratory and aircraft measurements. *Journal of Geophysical Research: Atmospheres*, *119*, 11,826–11,849. https://doi.org/10.1002/2014JD021848

McComiskey, A., Schwartz, S. E., Schmid, B., Guan, H., Lewis, E. R., Ricchiazzi, P., & Ogren, J. A. (2008). Direct aerosol forcing: Calculation from observables and sensitivities to inputs. *Journal of Geophysical Research*, *113*, D09202. https://doi.org/10.1029/2007JD009170

McMeeking, G. R., Fortner, E., Onasch, T. B., Taylor, J. W., Flynn, M., Coe, H., & Kreidenweis, S. M. (2014). Impacts of nonrefractory material on light absorption by aerosols emitted from biomass burning. *Journal of Geophysical Research: Atmospheres*, *119*, 12,272–12,286. https://doi.org/10.1002/2014JD021750

McMeeking, G. R., Kreidenweis, S. M., Baker, S., Carrico, C. M., Chow, J. C., Collett, J. L. Jr., et al. (2009). Emissions of trace gases and aerosols during the open combustion of biomass in the laboratory. *Journal of Geophysical Research*, *114*, D19210. https://doi.org/10.1029/2009JD011836

Melvin, M. (2015). National prescribed fire use survey report. Coalition of Prescribed Fire Councils.

Mitchell, R. J., Liu, Y., O'Brien, J. J., Elliott, K. J., Starr, G., Miniat, C. F., & Hiers, J. K. (2014). Future climate and fire interactions in the southeastern region of the United States. *Forest Ecology and Management*, *327*, 316–326. https://doi.org/10.1016/j.foreco.2013.12.003

NEI (2014). National emission inventory, US Environmental Protection Agency, available at: https://www.epa.gov/sites/production/files/2017-04/documents/2014neiv1_profile_final_april182017.pdf

Nikonovas, T., North, P. R. J., & Doerr, S. H. (2015). Smoke aerosol properties and ageing effects for northern temperate and boreal regions derived from AERONET source and age attribution. *Atmospheric Chemistry and Physics*, *15*, 7929–7943. https://doi.org/10.5194/acp-15-7929-2015

O'Dell, K., Ford, B., Fischer, E., & Pierce, J. (2019). The contribution of wildland-fire smoke to US PM2.5 and its influence on recent trends. *Environmental Science & Technology*, *53*(4), 1797–1804. https://doi.org/10.1021/acs.est.8b05430

Park, R. J., Jacob, D. J., Chin, M., & Martin, R. V. (2003). Sources of carbonaceous aerosols over the United States and implications for natural visibility. *Journal of Geophysical Research*, *108*(D12), 4355. https://doi.org/10.1029/2002JD003190

Peterson, D. A., Campbell, J. R., Hyer, E. J., Fromm, M. D., Kablick, G. P. III, Cossuth, J. H., & DeLand, M. T. (2018). Wildfire-driven thunderstorms cause a volcano-like stratospheric injection of smoke. *npj Climate and Atmospheric Science*, *1*(1), 30. https://doi.org/10.1038/s41612-018-0039-3

Pokhrel, R. P., Wagner, N. L., Langridge, J. M., Lack, D. A., Jayarathne, T., Stone, E. A., et al. (2016). Parameterization of single-scattering albedo (SSA) and absorption Ångström exponent (AAE) with EC/OC for aerosol emissions from biomass burning. *Atmospheric Chemistry and Physics*, *16*(15), 9549–9561. https://doi.org/10.5194/acp-16-9549-2016

Ramanathan, V., Crutzen, P. J., Kiehl, J. T., & Rosenfeld, D. (2001). Aerosols, climate, and the hydrological cycle. *Science*, *294*, 2119–2124. https://doi.org/10.1126/science.1064034

Ramnarine, E., Kodros, J. K., Hodshire, A. L., Lonsdale, C. R., Alvarado, M. J., & Pierce, J. R. (2019). Effects of near-source coagulation of biomass burning aerosols on global predictions of aerosol size distributions and implications for aerosol radiative effects. *Atmospheric Chemistry and Physics*, *19*(9). https://doi.org/10.5194/acp-2018-1084

Reid, C. E., Brauer, M., Johnston, F. H., Jerrett, M., Balmes, J. R., & Elliott, C. T. (2016). Critical review of health impacts of wildfire smoke exposure. *Environmental Health Perspectives*, *124*, 1334–1343. https://doi.org/10.1289/ehp.1409277

Reid, J. S., Eck, T. F., Christopher, S. A., Koppmann, R., Dubovik, O., Eleuterio, D. P., et al. (2005). A review of biomass burning emissions part III: Intensive optical properties of biomass burning particles. *Atmospheric Chemistry and Physics*, *5*(3), 827–849. https://doi.org/10.5194/acp-5-827-2005

Reid, J. S., Koppmann, R., Eck, T. F., & Eleuterio, D. P. (2005). A review of biomass burning emissions part II: Intensive physical properties of biomass burning particles. *Atmospheric Chemistry and Physics*, *5*(3), 799–825. https://doi.org/10.5194/acp-5-799-2005

Robock, A. (1988). Enhancement of surface cooling due to forest fire smoke. *Science*, *242*, 911–913.

Rolph, G. D., Draxler, R. R., Stein, A. F., Taylor, A., Ruminski, M. G., Kondragunta, S., et al. (2009). Description and verification of the NOAA smoke forecasting system: The 2007 fire season. *Weather Forecasting*, *24*(2), 361–378. https://doi.org/10.1175/2008WAF2222165.1

Ruminski, M., Kondragunta, S., Draxler, R. R., & Zeng, J. (2006). Recent changes to the hazard mapping system. In 15th International Emission Inventory Conference; 200621.

Russell, P. B., Bergstrom, R. W., Shinozuka, Y., Clarke, A. D., DeCarlo, P. F., Jimenez, J. L., et al. (2010). Absorption angstrom exponent in AERONET and related data as an indicator of aerosol composition. *Atmospheric Chemistry and Physics*, *10*(3), 1155–1169. https://doi.org/10.5194/acp-10-1155-2010

Sayer, A. M., Hsu, N. C., Eck, T. F., Smirnov, A., & Holben, B. N. (2014). AERONET-based models of smoke-dominated aerosol near source regions and transported over oceans, and implications for satellite retrievals of aerosol optical depth. *Atmospheric Chemistry and Physics*, *14*(20), 11,493–11,523. https://doi.org/10.5194/acp-14-11493-2014

Schlosser, J. S., Braun, R. A., Bradley, T., Dadashazar, H., MacDonald, A. B., Aldhaif, A. A., et al. (2017). Analysis of aerosol composition data for western United States wildfires between 2005 and 2015: Dust emissions, chloride depletion, and most enhanced aerosol constituents. *Journal of Geophysical Research: Atmospheres*, *122*, 8951–8966. https://doi.org/10.1002/2017JD026547

Schuster, G. L., Dubovik, O., & Holben, B. N. (2006). Angstrom exponent and bimodal aerosol size distributions. *Journal of Geophysical Research*, *111*, D07207. https://doi.org/10.1029/2005JD006328

Shi, S., Cheng, T., Gu, X., Guo, H., Wu, Y., & Wang, Y. (2019). Biomass burning aerosol characteristics for different vegetation types in different aging periods. *Environment International*, *126*, 504–511. https://doi.org/10.1016/j.envint.2019.02.073

Shi, Y. R., Levy, R. C., Eck, T. F., Fisher, B., Mattoo, S., Remer, L. A., et al. (2019). Characterizing the 2015 Indonesia fire event using modified MODIS aerosol retrievals. *Atmospheric Chemistry and Physics*, *19*, 259–274. https://doi.org/10.5194/acp-19-259-2019

Souri, A. H., Choi, Y., Jeon, W., Kochanski, A. K., Diao, L., Mandel, J., et al. (2017). Quantifying the impact of biomass burning emissions on major inorganic aerosols and their precursors in the U.S. *Journal of Geophysical Research: Atmospheres*, *122*, 12,020–12,041. https://doi.org/10.1002/2017JD026788

Spracklen, D. V., Mickley, L. J., Logan, J. A., Hudman, R. C., Yevich, R., Flannigan, M. D., & Westerling, A. L. (2009). Impacts of climate change from 2000 to 2050 on wildfire activity and carbonaceous aerosol concentrations in the western United States. *Journal of Geophysical Research*, *114*, D20301. https://doi.org/10.1029/2008JD010966

Sullivan, A. P., Guo, H., Schroder, J. C., Campuzano-Jost, P., Jimenez, J. L., Campos, T., et al. (2019). Biomass burning markers and residential burning in the WINTER aircraft campaign. *Journal of Geophysical Research: Atmospheres*, *124*, 1846–1861. https://doi.org/10.1029/2017JD028153

Sullivan, A. P., Holden, A. S., Patterson, L. A., McMeeking, G. R., Kreidenweis, S. M., Malm, W. C., et al. (2008). A method for smoke marker measurements and its potential application for determining the contribution of biomass burning from wildfires and prescribed fires to ambient PM2.5 organic carbon. *Journal of Geophysical Research*, *113*, D22302. https://doi.org/10.1029/2008JD010216

Sundarambal, P., Tkalich, P., & Balasubramanian, R. (2010). Impact of biomass burning on ocean water quality in southeast through atmospheric deposition: Eutrophication modeling. *Atmospheric Chemistry and Physics*, *10*(23), 11,337–11,357. https://doi.org/10.5194/acp-10-11337-2010

Vakkari, V., Kerminen, V. M., Beukes, J. P., Tiitta, P., van Zyl, P. G., Josipovic, M., et al. (2014). Rapid change in biomass burning aerosols by atmospheric oxidation. *Geophysical Research Letters*, *41*, 2644–2651. https://doi.org/10.1002/2014GL059396

Wagner, R., Jähn, M., & Schepanski, K. (2018). Wildfires as a source of airborne mineral dust - revisiting a conceptual model using large-eddy simulation (LES). *Atmospheric Chemistry and Physics*, *18*, 11863–11884. https://doi.org/10.5194/acp-18-11863-2018

Wang, J., & Christopher, S. A. (2006). Mesoscale modeling of Central American smoke transport to the United States: 2. Smoke radiative impact on regional surface energy budget and boundary layer evolution. *Journal of Geophysical Research*, *111*, D14S92. https://doi.org/10.1029/2005JD006720

Wang, J., Christopher, S. A., Nair, U. S., Reid, J. S., Prins, E. M., Szykman, J., & Hand, J. L. (2006). Mesoscale modeling of Central American smoke transport to the United States: 1. "Top-down" assessment of emission strength and diurnal variation impacts. *Journal of Geophysical Research*, *111*, D05S17. https://doi.org/10.1029/2005JD006416

Wang, J., van den Heever, S. C., & Reid, J. S. (2009). A conceptual model for the link between Central American biomass burning aerosols and severe weather over the south central United States. *Environmental Research Letters*, *4*. https://doi.org/10.1088/1748-9326/4/1/015003

Westerling, A. L., Hidalgo, H. G., Cayan, D. R., & Swetnam, T. W. (2006). Warming and earlier spring increase western U.S. forest wildfire activity. *Science*, *313*(5789), 940–943. https://doi.org/10.1126/science.1128834

Yao, J. Y., Brauer, M., Raffuse, S., & Henderson, S. B. (2018). Machine learning approach to estimate hourly exposure to fine particulate matter for urban, rural, and remote populations during wildfire seasons. *Environmental Science & Technology*, *52*(22), 13,239–13,249. https://doi.org/10.1021/acs.est.8b01921

Yokelson, R. J., Crounse, J. D., DeCarlo, P. F., Karl, T., Urbanski, S., Atlas, E., et al. (2009). Emissions from biomass burning in the Yucatan. *Atmospheric Chemistry and Physics*, *9*(15), 5785–5812. https://doi.org/10.5194/acp-9-5785-2009

Yue, X., Mickley, L. J., Logan, J. A., & Kaplan, J. O. (2013). Ensemble projections of wildfire activity and carbonaceous aerosol concentrations over the western United States in the mid-21st century. *Atmospheric Environment*, *77*, 767–780. https://doi.org/10.1016/j.atmosenv.2013.06.003